AGU PUBLICATIONS

Geochemistry, Geophysics, Geosystems

RESEARCH ARTICLE
10.1002/2017GC006922

The formation of gold-rich seafloor sulfide deposits: Evidence from the Beebe hydrothermal vent field, Cayman Trough

Alexander P. Webber[1], Stephen Roberts[1], Bramley J. Murton[2], Rachel A. Mills[1], and Matthew R. S. Hodgkinson[1,3]

[1]Ocean and Earth Science, National Oceanography Centre Southampton, University of Southampton, Southampton, UK, [2]National Oceanography Centre Southampton, Southampton, UK, [3]Natural History Museum, London, UK

Key Points:
- The Beebe vent field is forming an auriferous massive sulfide deposit with different gold concentrations in two different chimney types
- Beehive diffusers contain the most gold with precipitation of gold grains under reduced conditions in a pyrrhotite framework
- Beehive chimneys form through fluctuating pyrrhotite saturation during low effusive velocity venting

Supporting Information:
- Supporting Information S1
- Table S1

Correspondence to:
A. P. Webber,
a.webber@soton.ac.uk

Citation:
Webber, A. P., S. Roberts, B. J. Murton, R. A. Mills, and M. R. S. Hodgkinson (2017), The formation of gold-rich seafloor sulfide deposits: Evidence from the Beebe hydrothermal vent field, Cayman Trough, *Geochem. Geophys. Geosyst.*, *18*, doi:10.1002/2017GC006922.

Received 17 MAR 2017
Accepted 27 APR 2017
Accepted article online 8 MAY 2017

Abstract The Beebe vent field (BVF) in the Cayman Trough has built an auriferous massive sulfide deposit on the ultraslow spreading mid-Cayman spreading center. The genesis of auriferous sulfide deposits at mid-ocean ridges is not fully understood, although there is a growing recognition that slow and ultraslow spreading centers are conducive to gold mineralization. Analysis of hydrothermal precipitates from the BVF indicates that the highest gold contents are present within "beehive diffusers," which have developed a highly porous pyrrhotite framework. The beehive structure allows vent fluids to effuse slowly while allowing ingress of seawater to cool the fluid. The prevalence of pyrrhotite in the beehive samples, lack of sulfates, association between pyrrhotite and gold grains, and results of thermodynamic modeling suggest gold precipitation occurred under highly reduced conditions even during mixing with seawater. In contrast, high-temperature chimneys, with a single orifice, maintain high temperatures to the primary vent orifice and much of the gold is lost to seawater. Despite this, both chimney types are relatively gold-enriched, which points to a further underlying cause for high gold at the BVF such as interaction of hydrothermal fluids with ultramafic lithologies in the basement. The final gold composition of the deposit is partially controlled by loss of gold during mass-wasting of the material, with gold depletion most prevalent in blocks formed at beehive-type chimneys. The BVF demonstrates that the overall gold content of a massive sulfide deposit is the sum of basement, precipitation, and surface processes.

Plain Language Summary Mineral deposits form on the seafloor at hydrothermal vent sites and are rich in metals including copper, zinc, lead, and sometimes precious metals like gold and silver. However, the processes controlling the amount of gold that ends up in these deposits is not clearly understood. In this article we show that as hydrothermal fluid vents on the seafloor, two different types of chimney form. One is relatively gold-poor, while the other is gold-rich. The gold-rich chimneys, so-called "beehive" chimneys due to their appearance, are a very efficient structure for the formation of gold because the hot hydrothermal fluids are able to be cooled to much lower temperatures in the vicinity of the chimney. In comparison, the other type of chimney vents most of the gold to the ocean. Therefore, at this vent site, the formation of beehive chimneys may control the amount of gold in the deposit.

1. Introduction

Volcanogenic massive sulfide (VMS) deposits form at or near the seafloor as polymetallic sulfides precipitated from hot (up to ~400°C) hydrothermal fluids [*Franklin et al.*, 1981; *Jupp and Schultz*, 2000]. They form lenticular bodies rich in Cu, Zn, Pb, Ag, and Au dependent on tectonic setting, host rock lithology, and local precipitation mechanisms [*Galley et al.*, 2007; *Mercier-Langevin et al.*, 2015]. Approximately 9% of VMS deposits are classified as gold-rich, with more than 31 tons of contained gold at grades of greater than 3.46 g/t [*Mercier-Langevin et al.*, 2011]. The gold-rich VMS deposits are typically associated with calc-alkaline, intermediate to felsic host rocks, within a rifted-arc setting, addition of magmatic fluids, shallow emplacement leading to boiling, or postdepositional enrichment of gold grades [*Hannington et al.*, 1999; *Dubé et al.*, 2007]. However, auriferous deposits discovered at mid-ocean ridge settings, such as at the hydrothermal fields of TAG [*Hannington et al.*, 1995], Snakepit [*Fouquet et al.*, 1993], and recently the Beebe vent field (BVF) [*Webber et al.*, 2015] do not align with these associations.

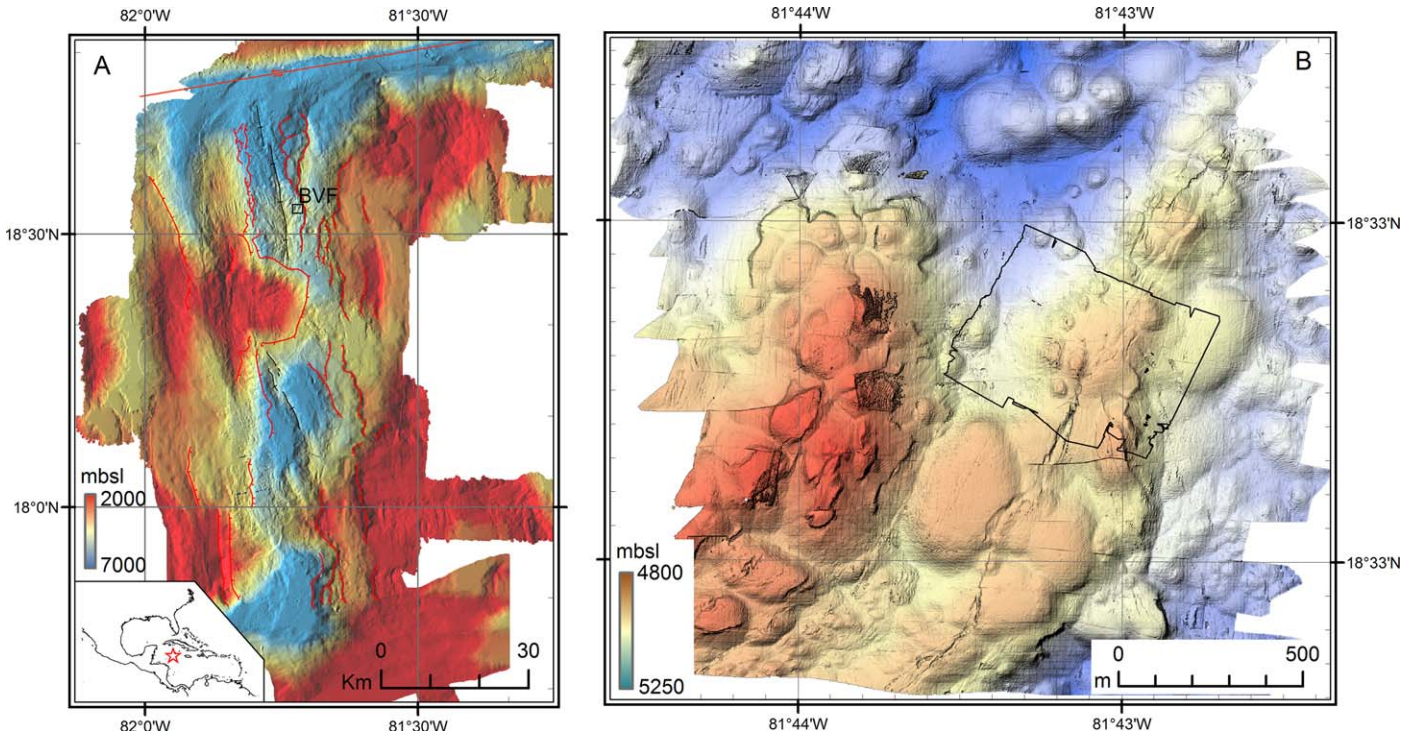

Figure 1. (a) Location of the Beebe Vent Field (BVF) in the Caribbean (inset) and on the mid-Cayman Spreading Centre (black square, which shows the extent of Figure 1b. The BVF is 3 km east of the spreading axis (black lines), on a volcanic ridge, which abuts a regional fault (red lines) 1 km to the east. (b) The area immediately surrounding the BVF comprises volcanic domes of basaltic pillow lavas. The BVF sits on the western flanks of a volcanic ridge, on the hanging wall side of a normal fault system which bisects the crest of the ridge. The black outline denotes the area covered by more detailed, 20 cm gridded bathymetry, available in *Webber et al.* [2015].

The BVF, in the Cayman Trough (Figure 1), is the World's deepest known hydrothermal vent system at 4960 m below sea level [*Connelly et al.*, 2012]. The BVF developed on basaltic crust at the ultraslow spreading Mid-Cayman Spreading Centre, and vents black smoker fluid at temperatures up to 401°C [*Webber et al.*, 2015]. The BVF is situated 3 km from the main ridge axis on a volcanic spur trending NE-SW. The spur is bisected along its length by a normal fault system, with a down throw of 13 m to the west. The BVF is located on the hanging wall of this fault system, on the western periphery of a ~500 m wide volcanic dome. It is composed of a series of 30–60 m wide sulfide mounds with mass-wasted sulfide sheets extending to the west. The BVF hosts two morphologically distinct groups of chimneys. The Beebe-125 and Hashtag chimneys are slender, up to ~30 cm wide, and vent the hottest fluids recorded (401°C) in a focused and vigorous style from the apex of each chimney (Figure 2a). They are composed primarily of copper sulfides, with chalcopyrite on the interior (Figure 2b), grading out to bornite ± chalcocite, followed by pyrite and anhydrite on the exterior. A second group of chimneys at Beebe Woods, 60 m to the south of Beebe-125, form a cluster of 30–100 cm thick "beehive" structures, up to 15 m tall (Figure 2c). These have a range of venting temperatures from shimmering water to ~350°C black smoker fluid. Samples of this chimney type show a lower-temperature mineral assemblage, with sphalerite, among a matrix of pyrrhotite, pyrite, and silica, with a highly porous pyrrhotite framework (Figure 2d). While both sets of chimneys contain a substantial amount of gold, ranging between 0.5 and 8 ppm Au at Beebe-125, the beehive chimneys of Beebe Woods contain considerably more gold ranging from 19 to 93 ppm Au [*Webber et al.*, 2015] (supporting information Table S1).

The difference in gold content between the two adjacent chimney types is striking. With no difference in end-member vent fluid composition between the two sites, it appears that chimney morphology and venting style could be a primary control on the differing gold concentrations. Here we show that the different vent morphologies and mineralogy can directly account for the difference in the gold contents, with efficient precipitation of gold at the Beebe Woods site producing highly gold-rich chimneys. Mixing with seawater under highly reduced conditions led to precipitation of gold at relatively high temperatures, and this process may contribute toward the formation of gold-rich VMS deposits. Furthermore, we show that the

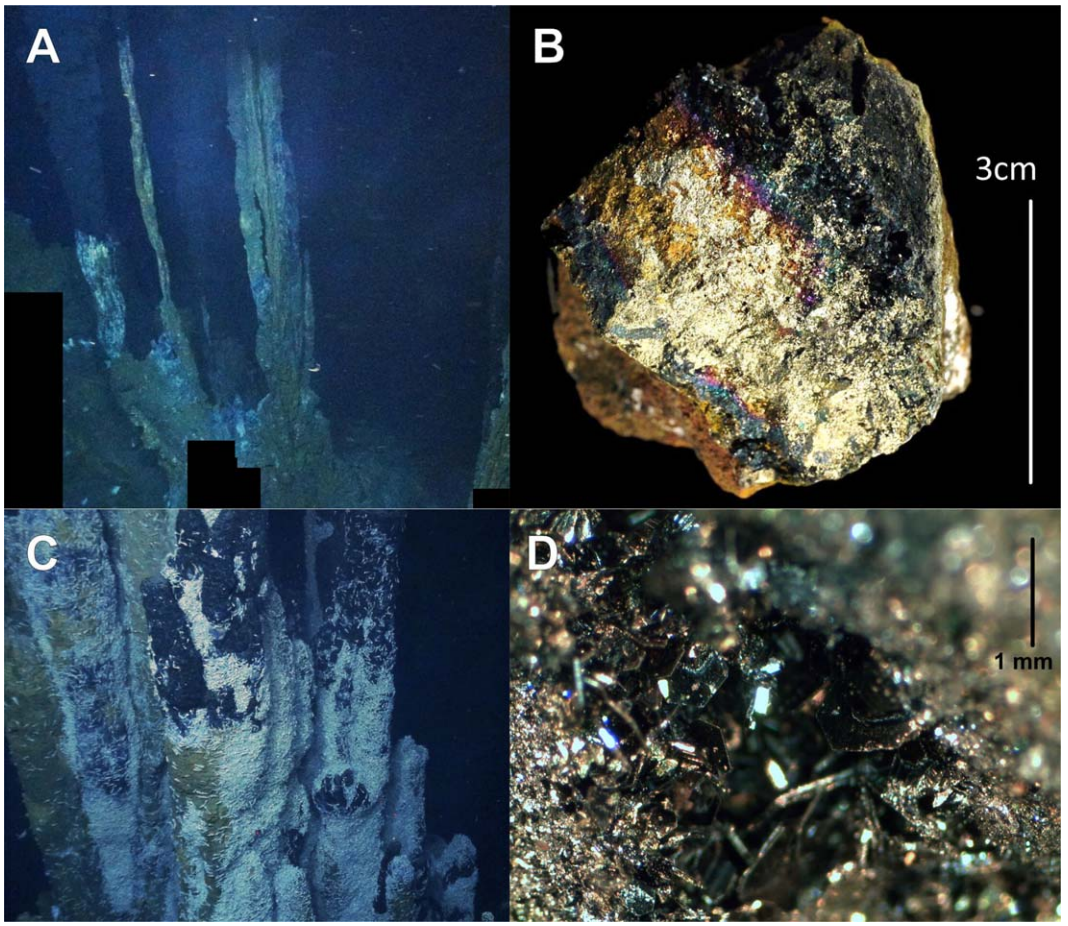

Figure 2. Examples of vent types and vent wall mineralogy. (a) High temperature, focused venting chimneys at Beebe-125 are 10–30 cm wide and are relatively gold-poor compared to beehive diffusers. (b) High-temperature, copper-rich chimneys produce interlocking copper minerals with low permeability, inhibiting fluid mixing. This example from the BVF is a ~3 cm wide solid chalcopyrite section of chimney wall. (c) Beehive diffusers at Beebe Woods, up to 1 m wide and 15 m tall. (d) Lower temperature, zinc, and iron sulfide-rich beehive chimneys produce permeable walls with millimeter-scale laths of pyrrhotite growing into open fluid pathways.

development of beehive-style chimneys is likely linked to the effusive velocity of venting leading to variable pyrrhotite saturation and a complex internal chimney structure. The underlying reason for the enhanced gold content across the BVF as a whole may be linked to interaction with ultramafic lithologies in the basement.

1.2. Previous Work

The following is a short summary of previous findings relevant to this work. Gold transport in seafloor hydrothermal fluids typically occurs under low to neutral pH, seawater-like salinity, high sulfidation, and moderately reducing conditions [*Hannington and Scott*, 1989a; *Benning and Seward*, 1996; *Seward and Barnes*, 1997; *Stefansson and Seward*, 2004]. In these settings, the $AuCl^-$ complex predominates at temperatures $>350°C$, with $Au(HS)_2^-$ and $AuHS_{(aq)}$ complexes more prevalent below this temperature at higher and lower pH, respectively. The solubility of gold in these solutions is dependent on temperature, pH, sulfur, and oxygen activity of the solution, and consequently, processes that influence these parameters control gold precipitation [*Hannington et al*., 1989b; *Pokrovski et al*., 2014]. For seafloor mineral deposits, these processes include cooling, mixing with seawater, sulfide precipitation, phase change (boiling), and wall-rock interaction. Within hydrothermal chimneys, mixing with seawater directly affects pH, temperature, sulfur, and oxygen activity and causes sulfide precipitation, while boiling can be important in relatively shallow environments. These observations are consistent with the highest gold concentrations usually occurring where mixing with seawater produces lower temperature diffuse, Zn-rich, "beehive," or "white smoker" chimneys [*Hannington et al*., 1986; *Fouquet et al*., 1993; *Herzig et al*., 1993; *Hannington et al*., 1995].

"Beehive" diffuser chimneys were first reported at the Snake Pit vent site at 23°N on the mid-Atlantic Ridge [*Fouquet et al*., 1993] where more diffuse, lower velocity flow was observed compared to focused chimneys. The Beehive diffusers lack a principle axial conduit, instead having a highly porous axial zone through which fluids diffuse to the top and laterally to the sides of the chimney; in this way they grow both upward and outward. These structures were reported to contain higher gold concentrations than the focused flow chimneys, with gold precipitation controlled primarily by the chimney morphology which allowed restricted seawater mixing on the margins of the chimney structure, in a relatively oxygen-rich regime, prior to pyrrhotite precipitation and close to the hematite-pyrite buffer. Similar structures and processes occur at other seafloor hydrothermal sites such as at the Lau Basin [*Herzig et al*., 1993] and TAG [*Hannington et al*., 1995].

At TAG, gold is concentrated in lower-temperature (265–300°C) "white smoker" chimneys on the periphery of the main mound [*Hannington et al*., 1995; *Thompson et al*., 1988]. In these chimneys, gold concentrations reached 42.4 ppm and were strongly associated with dendritic, Fe-poor sphalerite. Gold precipitation in the white smoker chimneys was largely attributed to the precipitation of sulfides leading to decreased H_2S and more oxygen-rich conditions, coupled with the ability of the $Au(HS)_2^-$ complex to remain stable to low temperatures. However, as a discrete gold-rich phase was not identified in the active chimneys, the gold was assumed to be present as submicroscopic particles within sphalerite aggregates or adsorbed onto mineral surfaces, or in solid solution within sulfides. Consequently, gold precipitation by adsorption onto mineral surfaces, which occurs independently of gold saturation state, was considered an important mechanism for gold precipitation in white smokers, where the processes would be enhanced by the high internal surface area of the chimneys provided by the dendritic sphalerite, and comparatively long residence time of the fluid within the chimney.

Once gold-rich precipitates have formed, the final gold content of the seafloor sulfide deposit may depend on secondary processes that occur at the surface and interior of the mound. At the surface of the deposit, gold present within sulfides can be lost to dissolution by seawater as those sulfides are oxidized [*Hannington et al*., 1988]. Gold has also been described as part of the zone-refining model for the distribution of Cu and Zn within VMS deposits and seafloor sulfide mounds [*Eldridge et al*., 1983; *Hekinian et al*., 1985; *Hekinian and Fouquet*, 1985; *Hannington et al*., 1986, 1995; *Huston and Large*, 1989; *Huston*, 2000]. As talus is incorporated into the mound, gold is remobilized by circulating fluids which then vent at white smoker sites, leading to the formation of gold-rich zones at the top of the deposit. However, this reprocessing has been suggested to lead to a gold-poor deposit, as a large proportion of the reworked gold is vented on each occasion [*Hannington and Scott*, 1989b]. However, at PACMANUS in the Manus Basin, a felsic-hosted system, significant reworking of gold in the subsurface was not observed [*Ihle et al*., 2005].

2. Methods

Samples of sulfide chimneys from the Beebe vent site were collected on cruise JC82 with the *ISIS* remotely operated vehicle. Samples were subsequently dried, cut for thin section, and a portion ground to a powder for analysis. Fe, Cu, and Zn were analyzed by inductively coupled plasma atomic emission spectroscopy (ICP-AES), other elements by inductively coupled plasma mass spectrometry (ICP-MS). Sulfides were examined under reflected light and analyzed using a LEO1450VP variable pressure scanning electron microscope (SEM), with an X-Act, 10 mm^2 area silicon drift detector, energy dispersive X-ray spectroscopy (EDS). Samples of vent fluid were collected from the BVF with gas-tight samplers and analyzed with ion chromatography, ICP-MS, and ICP-AES. To explore the gold precipitation, thermodynamic modeling was undertaken with Geochemist's Workbench, using the internally consistent values of *Akinfiev and Zotov* [2010] and evaluated by *Pokrovski et al*. [2014], combined with the Au-hydroxide values from *Pokrovski et al*. [2014]. DBCreate [*Kong et al*., 2013], which in turn uses SUPCRT92 [*Johnson et al*., 1992], was used to create a thermodynamic database for the prevailing conditions at Beebe: 500 bar and 0–400°C. Modeling was undertaken under two conditions, one where no minerals are present initially, and the fluid composition reflects the measured values. The second reflects buffered conditions, which is likely to be more realistic of a hydrothermal fluid flowing diffusely through a chimney with a very high internal surface area, such as within the beehive chimneys. Given the sulfides present in the analyzed chimneys are mainly pyrrhotite and pyrite, indicating reduced conditions, the fluid is buffered with these two minerals. In this highly dynamic system of hydrothermal chimney growth, we do not attempt to take account of kinetic effects, and equilibrium modeling

should be approached with caution. However, the results presented here should give an indication as to the state that the system is working toward, for example, gold precipitation rather than dissolution.

3. Results

3.1. Vent Fluid Chemistry

Vent fluid samples were collected from chimney orifices using gas tight syringes and screened using the Mottl VentDB criteria. All data presented here (Table 1) meet these criteria (Mg-Ca $r^2 = 0.97$, $n = 10$). End-member chloride content is 362 mmol kg^{-1} and a common source fluid is inferred for the whole BVF based on the covariance of Mg with Cl, Ca, and Na across the three discrete venting sites sampled (supporting information Figure S1). Beehive diffusers are notoriously difficult to sample without entraining chimney fragments and all samples from Beebe Woods suffered from this artifact, leading to anomalously high metal contents in each sample. Excluding samples on the basis of entrainment of chimney material rich in Fe, Cu, Zn, and other metals demonstrates that only fluids collected at Beebe-125 are free from such artifacts. End-member fluid data for these samples indicate that Beebe vent fluids are Cu (112 mmol kg^{-1}) and Fe (6640 mmol kg^{-1}) rich with elevated H_2S (3.7 mmol kg^{-1}) and depleted Cl (362 mmol kg^{-1}). These fluids are inferred to form at high temperature and pressure from super critical phase separation by generation of a vapor-rich, low-chlorinity phase that is enriched in metals and H_2S. Gold determinations in BVF fluids are all impacted by entrainment of chimney particulates that are rich in gold.

3.2. Occurrence of Gold

At the Beebe Woods vent site, gold occurs as discrete, amorphous, 1–10 μm sized grains of gold and gold alloys (Figure 3). These grains occur in a variety of locations, often on the edges of grain boundaries of pyrrhotite and iron oxides (Figure 3b). They are sometimes enclosed within pyrrhotite and iron oxide, and only once seen within chalcopyrite, as a series of discrete inclusions and gold-rich domains (Figure 3c). Discrete gold grains are absent in proximity to fluid conduits, which are 1–20 mm scale voids into which euhedral pyrrhotite has grown. The gold occurs either as native grains, as electrum with 8–13% Ag, or rarely alloyed with 52–60% Sb (Table 2). Gold grains were not observed in the higher-temperature chimney samples.

3.3. Thermodynamic Modeling

Thermodynamic modeling used the end-member fluid compositions of the BVF vent fluid, conventionally established [*Von Damm et al*., 1985] by extrapolation of vent fluid analyses to zero magnesium (Table 1). We use an estimate of the end-member gold concentration in order to explore the behavior of gold in the BVF fluid, based on estimated gold concentrations in fluids at other sites of 0.0003–0.001 μmol/kg [*Hannington et al*., 2005]. The different gold concentrations do not greatly affect the results, with only a ~20°C difference in the gold saturation temperature between these high and low concentrations. For the following simulations we use 0.001 μmol/kg. Using this value, the end-member fluid is severely under-saturated with respect to gold at 400°C and is capable of dissolving around 4 orders of magnitude more gold.

Under conductive cooling conditions (Figure 4), $AuCl_2^-$ is the dominant species from 400 to 350°C (Figure 4a). Below this, $AuHS_{(aq)}$ is the main gold species. In the absence of any mineral buffers, gold saturation is not reached until ~40°C (Figures 4c and 4e). In the presence of a pyrite-pyrrhotite buffer from 400°C, which keeps the fluid highly reduced, $AuHS_{(aq)}$ is the primary gold species above 150°C, and below this temperature gold is evenly complexed as $AuHS_{(aq)}$ and $Au(HS)_2^-$ (Figure 4b). In this model, gold saturation occurs at ~140°C (Figures 4d and 4f). If the hydrothermal fluid is cooled by mixing with seawater (Figure 5), gold speciation results are similar to the conductive cooling model except the molar concentrations trend to lower values due to dilution by seawater. The temperature at which $Au(HS)_2^-$ becomes equal to $AuHS_{(aq)}$ is slightly lower at 125°C under buffered conditions (Figure 5b) but the temperature at which gold becomes stable is similar to the conductive mixing model (Figures 5d and 5f).

The behavior of the copper minerals gives a strong indication as to which model is the most realistic. If the fluid is not buffered by the presence of pyrite or pyrrhotite, chalcopyrite does not reach saturation until ~275°C and the primary copper mineral is bornite (Figures 4c and 5c), which is not consistent with the observation that the high-temperature (400°C) chimneys are lined with chalcopyrite. Under pyrite-pyrrhotite buffered conditions, chalcopyrite is stable at 400°C and the sequence of copper mineral precipitation, from high to low temperature, matches the observed sequence of copper minerals from inside to

AGU Geochemistry, Geophysics, Geosystems

10.1002/2017GC006922

Table 1. Vent Fluid Data of BVF Fluid Samples[a]

Sample	Vent Site	Depth (m)	Max Temp (°C)	pH	Na (mmol/kg)	Mg (mmol/kg)	Si (mmol/kg)	Cl (mM)	K (mmol/kg)	Ca (mmol/kg)	Li (μmol/kg)	Mn (μmol/kg)	Fe (μmol/kg)	Cu (μmol/kg)	Zn (μmol/kg)	Rb (μmol/kg)	Sr (μmol/kg)	Cs (μmol/kg)	Ba (μmol/kg)	Pb (μmol/kg)	SO_4 (mM)	H_2S (mM)
FLU13	Beebe 125	4,960	401	3.09	314	2.61	37[a]	371	9.93	7.01	345	569	6,600	218[a]	87.5	24.8	4.89	0.115	35.3[a]	0.452[a]	3.28	0.27
FLU14	Beebe 125	4,960	401	6.08	435	45.1	4.75	541	9.84	9.73	58.5	56.3	606	22.3	7.81	80.5	2	0.0125	0.646	0.0393	24.2	4.66
FLU15	Beebe 125	4,960	401	5.98	410	41.1	6.48	541	9.41	9.18	77	89.9	824	17.1	6.83	73.8	1.92	0.0125	1.36	0.0315	23.1	1.81
FLU16	Hashtag	4,970		2.91	322	5.41	38.6[a]	382	9.95	7.1	331	540	6,490	343[a]	77.5	27	4.6	0.107	5.59	0.423[a]	4.46	5.13
FLU17	Hashtag	4,970		2.99	327	9.69	37.9[a]	396	9.93	7.5	303	488	8,220[a]	1,560[a]	74.4	32.1	3.95	0.0937	3.65	0.34[a]	6.03	6.87
FLU18	Hashtag	4,970		3.42	361	21.5	23.5[a]	444	9.66	9.94[a]	233	367	17,800[a]	3,320[a]	478[a]	58.4[a]	3.72	0.0583	2.45	3.01[a]	15.3	3.7
FLU20	Beebe Woods	4,960	354	3.51	379	26.7	7.01	465	10	10.1[a]	191	273	29,000[a]	4,670[a]	660[a]	67[a]	2.75	0.0524	2.16	2.46[a]	16.5	2.57
FLU21	Beebe Woods	4,960	354	4.75	413	39.1	2.98	508	9.68	16.4[a]	102	130	51,800[a]	10,200[a]	681[a]	117[a]	2.04	0.0238	1.62	2.78[a]	40.2[a]	4.4
FLU22	Beebe Woods	4,960	354	4.31	403	35.1	6.61	497	9.92	8.95	135	181	23,500[a]	9,270[a]	73.3[a]	67.7	2.31	0.0312	1.37	0.12	21.4	1.9
FLU23	Beebe 125	4,960	401	3.05	319	2.03	23.6	372	10.3	6.76	360	574	6,290	117	39	24.3	4.47	0.111	20.2[a]	0.224	3.07	4.22
FLU24	Beebe 125	4,960	401	3.86	400	33.8	7.5	499	10	8.67	144	196	1,980	60	22.6	64.7	2.27	0.0372	1.57	0.0976	18.2	1.31
FLU25	Beebe 125	4,960	401	3.06	320	5.64	21.6	388	10.1	6.82	330	515	5,580	105	58.8	28	3.96	0.106	6.79	0.233	4.66	3.15
FLU26	Beebe 125	4,960	401	3.04	301	2.98	22	378	9.59	6.4	327	524	5,700	89.8	52.2	23.9	3.92	0.104	7.04	0.186	3.52	3.22
End-member[b]					304	0	23.4	362	10	6.61	366	594	6,640	112	53.5	20.5	4.62	0.117	6.41	0.231	2.01	3.66

[a]Values show evidence for contamination by particles during sampling and were excluded from end-member calculations.
[b]End-member values calculated by extrapolation to 0 magnesium.

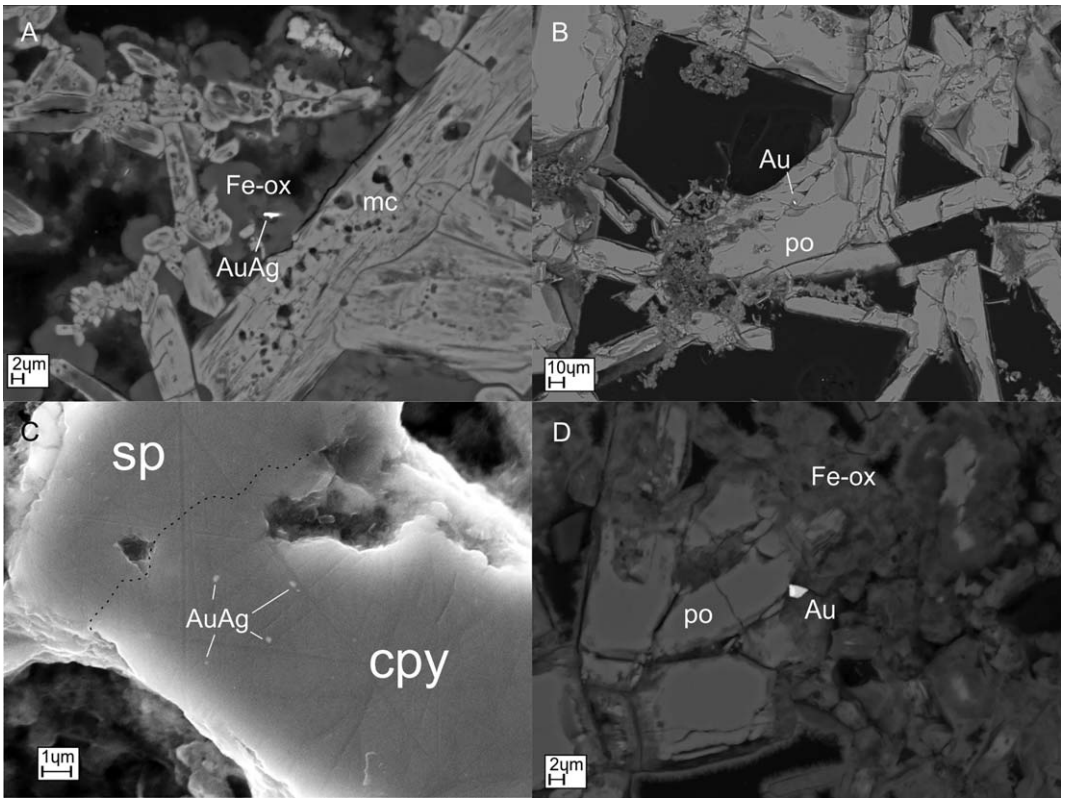

Figure 3. SEM images of gold grains found in samples from Beebe Woods. (a) Lath-like gold enclosed within iron oxide on the boundary of altered marcasite. (b) Gold enclosed within pyrrhotite. A high proportion of pore space is visible. (c) Gold-rich areas within chalcopyrite-sphalerite grain. The grain boundary has been marked for clarity. (d) Gold grain on pyrrhotite and iron oxide boundary. mc is marcasite, po is pyrrhotite, sp is sphalerite, cpy is chalcopyrite, Fe-ox is iron oxide.

out in the chimney samples; chalcopyrite followed by bornite then chalcocite (Figures 4d and 5d). In addition, the close association between pyrrhotite and the inclusions of gold suggest the fluid is highly reduced during gold precipitation (Figure 6).

The pyrite-pyrrhotite buffer controls the temperature at which gold reaches saturation. If no minerals are present, and none are allowed to precipitate in the model (the fluid is not buffered), gold does not reach saturation until ~30–40°C (Figures 4c and 5c). In the presence of a pyrite-pyrrhotite buffer, however, gold precipitates at temperatures of ~140°C (Figures 4d and 5d). If pyrrhotite is present throughout the entire mixing regime, the temperature at which gold precipitates is maximized because gold is stable at higher temperatures in more reduced conditions (Figures 7a–7d). However, if the quantity of pyrrhotite is limited, it can be totally consumed and the fluid is allowed to depart from the pyrite-pyrrhotite buffer, leading to more oxidized conditions and, as long as $SO_4/H_2S < 1$, a lower temperature of gold formation. This scenario leads to the possibility that gold can be remobilized by flushing through a more oxidized fluid at similar or higher temperatures, or by the growth of the chimney allowing gold particles to interact with fluid at higher temperatures. There is evidence for gold interacting with higher-temperature fluids in the

Table 2. EDS Results for Gold Blebs[a]

	Alloying Elements		
Spectra	Ag	Au	%Ag
1	6.93	48.3	13%
2	5.5	40.32	12%
3	3.51	31.17	10%
4	2.81	24.31	10%
5	2.73	24	10%
6	1.56	16.32	9%
7	1.46	16.2	8%
8	1.41	9.88	12%
9	0.87	9.8	8%
	Sb	Au	%Sb
10	4.05	3.74	52%
11	3.87	2.68	59%
12	3.41	2.32	60%

[a]Results of EDS analysis of individual gold alloy inclusions. The inclusions were chemically defined in three groups; pure gold (18) – not shown, Au-Ag alloy (9), and Au-Sb alloy (3).

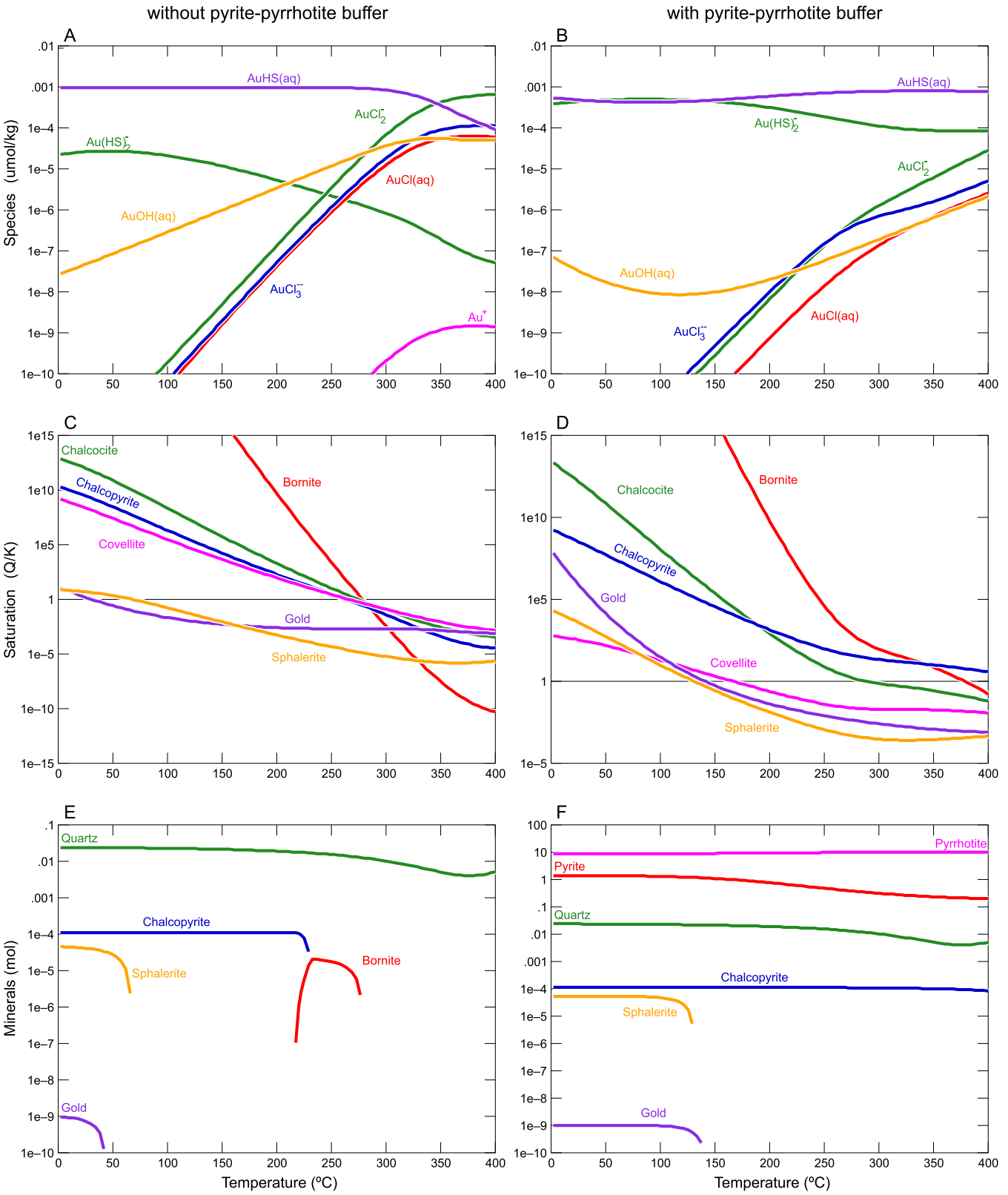

Figure 4. Results of thermodynamic calculations, where BVF fluid is conductively cooled from 400 to 2°C. Figures 4a and 4b show results of Au speciation, Figures 4c and 4d show mineral saturation without mineral precipitation, and Figures 4e and 4f show minerals present where precipitation is allowed. The left-hand figures are performed without a mineral buffer present, and the right-hand figures are performed with pyrite and pyrrhotite present in sufficient quantities to exist through the entire reaction path. Note that the saturation and precipitation of the copper-sulfides is more realistic under buffered conditions, and the temperature of gold precipitation is raised from ~75 to ~175°C.

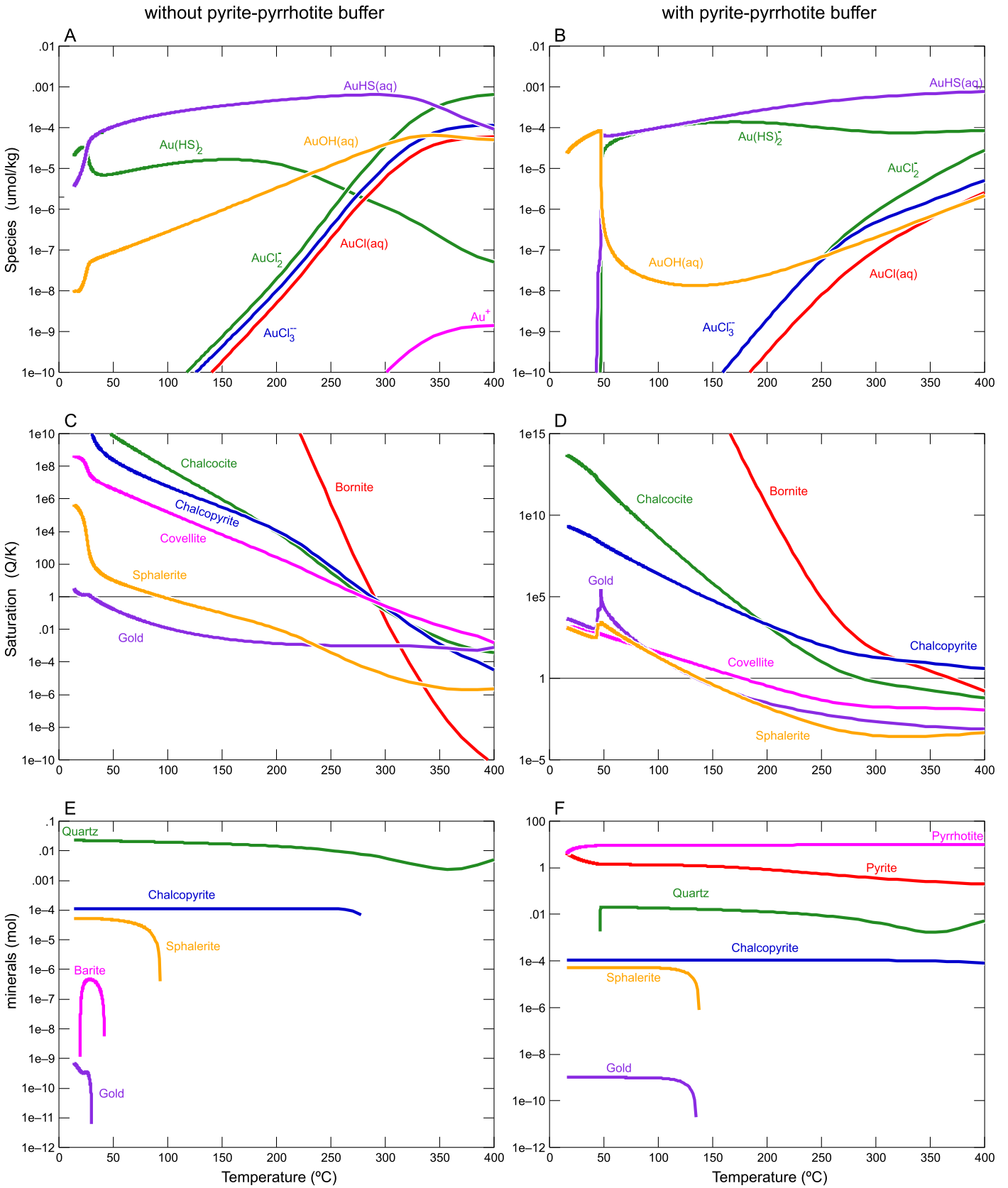

Figure 5. Results of thermodynamic calculations, as in Figure 4, except cooling is achieved by mixing with ambient seawater.

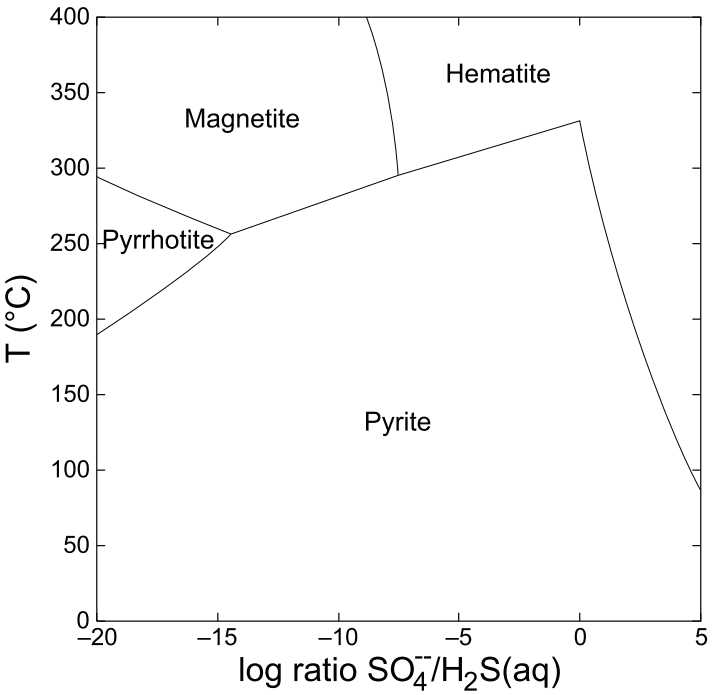

Figure 6. The stability of iron phases at 500 bar, log SO_4^{2-} activity = −3, log Cl^- activity = −0.5, O_2 activity is expressed as SO_4^{2-}/H_2S. The availability of pyrite and pyrrhotite to the fluid will buffer the fluid to very low oxygen activities.

form of gold-rich domains in chalcopyrite and sphalerite overgrown by chalcopyrite (Figure 3c).

Under conditions commonly found at black smoker sites, with moderate to low pH, gold stability is affected strongly by both the oxidation and pH of the fluid (Figure 7). Maintaining log $SO_4/H_2S < 0$ results in a generally lower temperature at which gold precipitates but that temperature increases with decreasing SO_4/H_2S (Figures 7c and 7d). Under more oxidized conditions, gold stability occurs at temperatures as high as 250°C, and the pH of the fluid has comparatively little effect.

4. Discussion

4.1. Precipitation of Gold

The results of the thermodynamic modeling are consistent with the observation that chimney morphology at the BVF strongly influences the gold content of the vent site. At Beebe-125 and Hashtag, hydrothermal fluid at 400°C or greater, well above the stability temperature of gold, is transported rapidly along primary fluid conduits to the apex of the chimneys, with little opportunity for the precipitation of gold in the chimney walls. The chalcopyrite inner walls, which are relatively impermeable, limit the amount of fluid that can pass into the more permeable, lower-temperature anhydrite-pyrite portion of the wall. At Beebe Woods, however, the high permeability of the chimney walls and large quantity of smaller fluid conduits has allowed much more of the fluid to experience lower temperatures. The sphalerite-rich mineralogy of these chimneys suggests that the fluid regularly reaches temperatures lower than 150°C (e.g., Figure 4d). Furthermore, the quantity of pyrite and pyrrhotite in these chimneys and the amount of pore space surrounding these phases suggest the fluid composition is kept close to the pyrite-pyrrhotite buffer, which raises the temperature at which gold can precipitate (Figure 7). This finding is contrary to most other studies of gold-rich chimneys at hydrothermal sites, which instead attribute gold precipitation under oxygen-rich conditions by mixing with seawater, close to the hematite-pyrite buffer [*Herzig et al*., 1993; *Fouquet et al*., 1993; *Hannington et al*., 1995] and prior to pyrrhotite precipitation [*Fouquet et al*., 1993]. This may be true for white smoker chimneys, which show evidence of mixing with seawater in the mound prior to entering the chimney and which contain abundant sulfates such as anhydrite and barite. Under these conditions, the fluid is likely to intersect the gold stability boundary where $SO_4/H_2S > 1$. We find no evidence for this at the BVF. Instead, the abundance of pyrrhotite at Beebe Woods, general lack of anhydrite or other sulfates, and the venting of typical black smoker fluids, suggests that the fluid precipitating gold is close to the pyrite-pyrrhotite buffer under highly reduced conditions. The modeling suggests these reduced conditions can be maintained up to very high degrees of seawater mixing, until the complete consumption of pyrrhotite occurs. In the higher-temperature, copper-rich chimneys, lower temperatures only exist in the relatively impermeable walls of the chimneys, but under much more oxidized conditions, as evidenced by the prevalence of a pyrite-anhydrite assemblage. As a result, a much lower proportion of the fluid experiences conditions suitable for gold precipitation, and the gold content of these chimneys is lower. However, it is not clear which type of chimney precipitates the greater net quantity of gold, given the differing fluid flow rates and chimney growth rates. If a vastly higher quantity of fluid is vented by the higher-temperature chimneys, they may precipitate as much or more gold than the beehive chimneys, albeit at a lower overall grade.

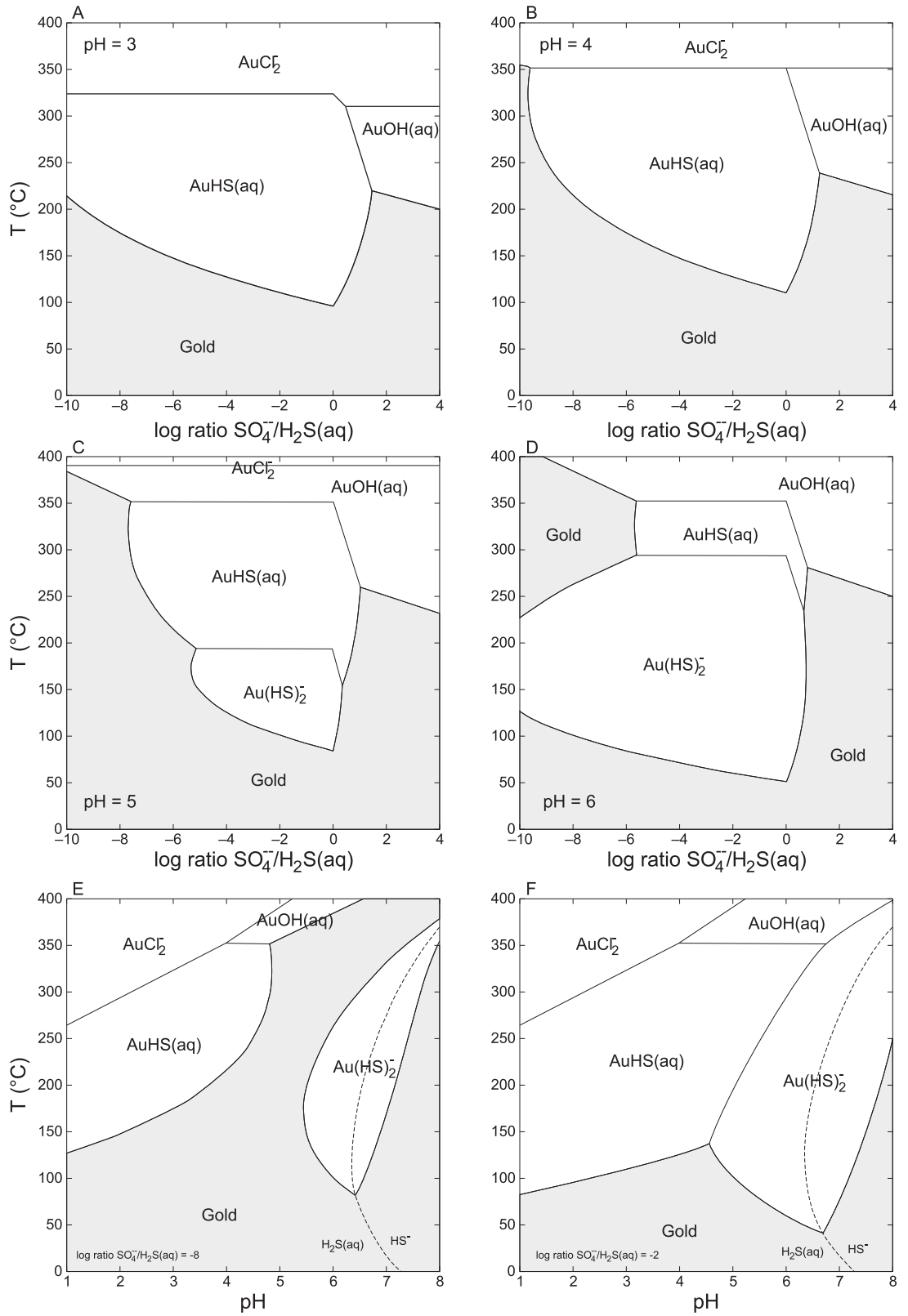

Figure 7. Speciation diagrams for Au at 500 bar, log SO_4^{2-} activity = −3, log Cl^- activity = −0.5, O_2 activity is expressed as SO_4^{2-}/H_2S. Figures 7a through 7d demonstrate how Au speciation varies with O_2 at differing pH. When log $SO_4^{2-}/H_2S < 0$, more reduced fluids tend to precipitate gold at higher temperatures. Figures 7e and 7f explore the variation of pH, which strongly controls the speciation. More acidic solutions carry gold as $AuCl_2^-$ and AuHS(aq), while alkaline solutions carry gold as $Au(HS)_2^-$. Sulfide is speciated over pH. Diagrams adapted from *Cleverley and Bastrakov* [2005].

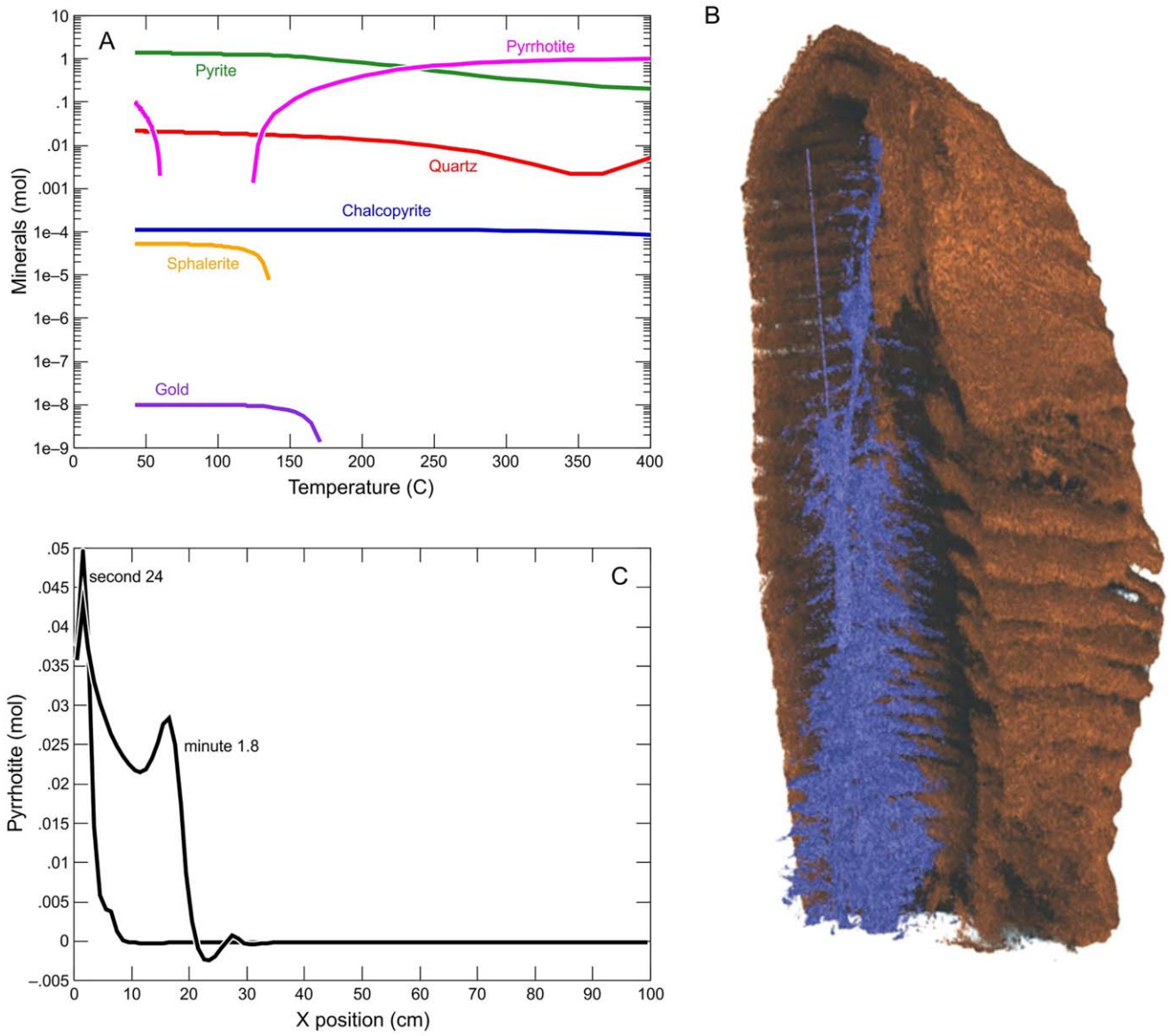

Figure 8. (a) Mixing between 400°C Beebe vent fluid and 4°C seawater, with an initial 1 mol of pyrrhotite present. At ~130°C, all of the pyrrhotite has been consumed (either dissolved or replaced by pyrite); however, at temperatures less than 60°C it is again saturated. This fluctuating pyrrhotite saturation may lead to the development of rib-like structures. (b) CT scan of a beehive chimney (12 cm diameter by 18 cm high) from the Moytirra vent field, 45°N mid-Atlantic Ridge [*Wheeler et al*., 2013], showing internal rib structures. The beehive chimney has been imaged using a 450 kV Hutch Nikon/Metris custom-designed hard X-ray CT-scanner at the m-Vis facility, University of Southampton. Making the medium-density material invisible reveals the internal structure, comprising alternating bands or ribs of sulfide material (brown) separated by lower-density anhydrite rich areas (invisible). By highlighting the pore space (blue) the internal fluid pathways are also made visible revealing an internal vertical pipe-like structure within the beehive chimney. (c) A one-dimensional flow-through model where 400°C Beebe vent fluid is replacing 4°C seawater. After 24 s, an initial ridge of pyrrhotite is produced, and behind this ridge is an area with less pyrrhotite. After 1.8 min, three ridges of pyrrhotite have developed, similar to the internal structure of beehive chimneys.

4.2. Formation of the Beehive Chimneys

The thermodynamic modeling showed that a complex interplay exists between pyrrhotite, pyrite, and gold precipitation when seawater is used to cool the hydrothermal fluid. By buffering the fluid, the amount of pyrrhotite available controls the temperature at which gold precipitates, and pyrrhotite itself can be totally consumed in this process (Figure 8a). However, as the mixing with seawater continues, at lower temperatures pyrrhotite saturation increases and can reprecipitate (Figure 8a). The beehive chimneys contain complex structures, with regular, horizontal rib-like pore spaces that allow lateral flow of fluids toward the chimney walls [*Fouquet et al*., 1993]. The structure and high porosity can be seen clearly on a CT scan of a beehive chimney (Figure 8b). We suggest this structure may be the result of fluctuations in

pyrrhotite saturation. As the vent fluid moves through the chimney structure and ultimately mixes with seawater, pyrrhotite is replaced with pyrite and other sulfides, and quartz and anhydrite are precipitated at moderate (100–200°C) temperatures. Below ~130°C, few minerals are precipitated until the fluid reaches 60°C, when pyrrhotite is again precipitated (Figure 8a). A one-dimensional flow-through model can recreate this phenomenon, producing an initial "ridge" of pyrrhotite, followed by a trough as the pyrrhotite is dissolved, before another ridge of pyrrhotite is formed (Figure 8c). These ridges and troughs of pyrrhotite in the fluid mixing model may be analogous to the ribs and fluid pathways in the beehive chimney. At the apex of the chimney, cooling by mixing with seawater results in pyrrhotite precipitation, but fluid flow must be slow enough to allow large degrees of mixing, in order to reach ~60°C, across the width of the chimney. This is consistent with previous work that has linked effusive velocity to chimney morphology [*Fouquet et al*., 1993]. The pyrrhotite occurs as millimeter-scale hexagonal plates (Figure 2b), creating an open structure with a high proportion of pore space. This structure encourages higher degrees of seawater mixing, development of the rib-like structures, lower-velocity venting over a wider proportion of the chimney, and thus the process is self-perpetuating. In contrast, more focused, higher-velocity venting, perhaps from an individual fissure rather than a wider area of sulfide talus, would inhibit seawater mixing, maintaining higher temperatures and therefore the prevalence of interlocking copper minerals, which create an impermeable barrier to further seawater mixing (Figure 2a). Lower-velocity venting would lead to higher degrees of seawater mixing and therefore lower temperatures in proximity to the existing chimney structure. Since lower temperatures are required to precipitate, rather than consume pyrrhotite, this would lead to pyrrhotite precipitation.

4.3. Mass Wasting

The BVF is built on the side of a steeply sloping edifice of pillow lavas, and mass wasting of the sulfide is a prominent feature of the deposit. Talus spreads westward from the BVF in fans which extend up to 200 m from the vent sites, with finer sand and mud-sized particles extending even further [*Webber et al*., 2015]. The talus is highly recrystallized, showing little evidence for chimney structures at the hand specimen scale and is severely depleted in Cu and Zn compared to the zero-age chimneys (Figure 9a). However, the behavior of gold during weathering is less clear, with some talus samples being relatively high in gold compared to chimneys (Figure 9b). When the talus material is grouped by their Cu and Zn content, it is possible to infer which type of vent that talus material came from, focused chimneys, and beehives having high Cu/Zn compared to low Cu/Zn, respectively (Figure 9a). This allows some assessment of the mobility of elements in the two types of talus. Certain elements behave as expected; addition of Mn and loss of Ca is consistent between both chimney types, for example (Figures 9b and 9c). But gold exhibits very different behavior depending on which type of vent the sample was formed at. Beehive chimneys seem to have lost gold, with the scaled isochron diagram indicating it has a similar mobility to Ca, Cu, Zn, Al, and Ag (Figure 9b). However, the high-temperature chimneys show much less evidence for gold loss, appearing to behave similarly to Cr and Zr (Figure 9c). This seems to suggest that gold is less available for reaction or loss from talus created from high-temperature chimneys than beehives, perhaps due to lower permeability and surface area. Gold dissolution from altered seafloor sulfides has previously been reported [*Hannington et al*., 1988]. The release of lattice-bound and fine-grained gold from weathering sulfides is one possible way to get gold into seawater quickly. In addition, there is likely to be a physical removal of nanoscale gold particles at least from the exterior of talus blocks, with particles being either washed away or preserved within finer sediments that were not sampled.

The amount of gold preserved in the mass-wasted material is likely to be related to the grain size distribution of the talus, which in turn is linked to the distance the clasts have travelled from the vent site. As blocks are transported, they will be broken, increasing surface area, releasing gold particles and exposing fresh crystal faces to seawater. More proximal deposits should contain more gold than those found distally. This process is controlled by the terrain on which the deposit forms; flatter terrain will lead to a shorter transport distance, thicker talus beds, and therefore more gold preserved. Steep terrain, like that found at the BVF, leads to longer transport distances, a finer grain size distribution, thinner talus beds, and therefore less gold preserved. Similar conclusions can be reached for the Cu and Zn content of the talus. Although the mound talus appears to have lost gold, it retains a high gold content in comparison to other VMS ores and seafloor sulfides. With 0.5–15 ppm Au, they would form a gold-rich horizon that would otherwise be described as a

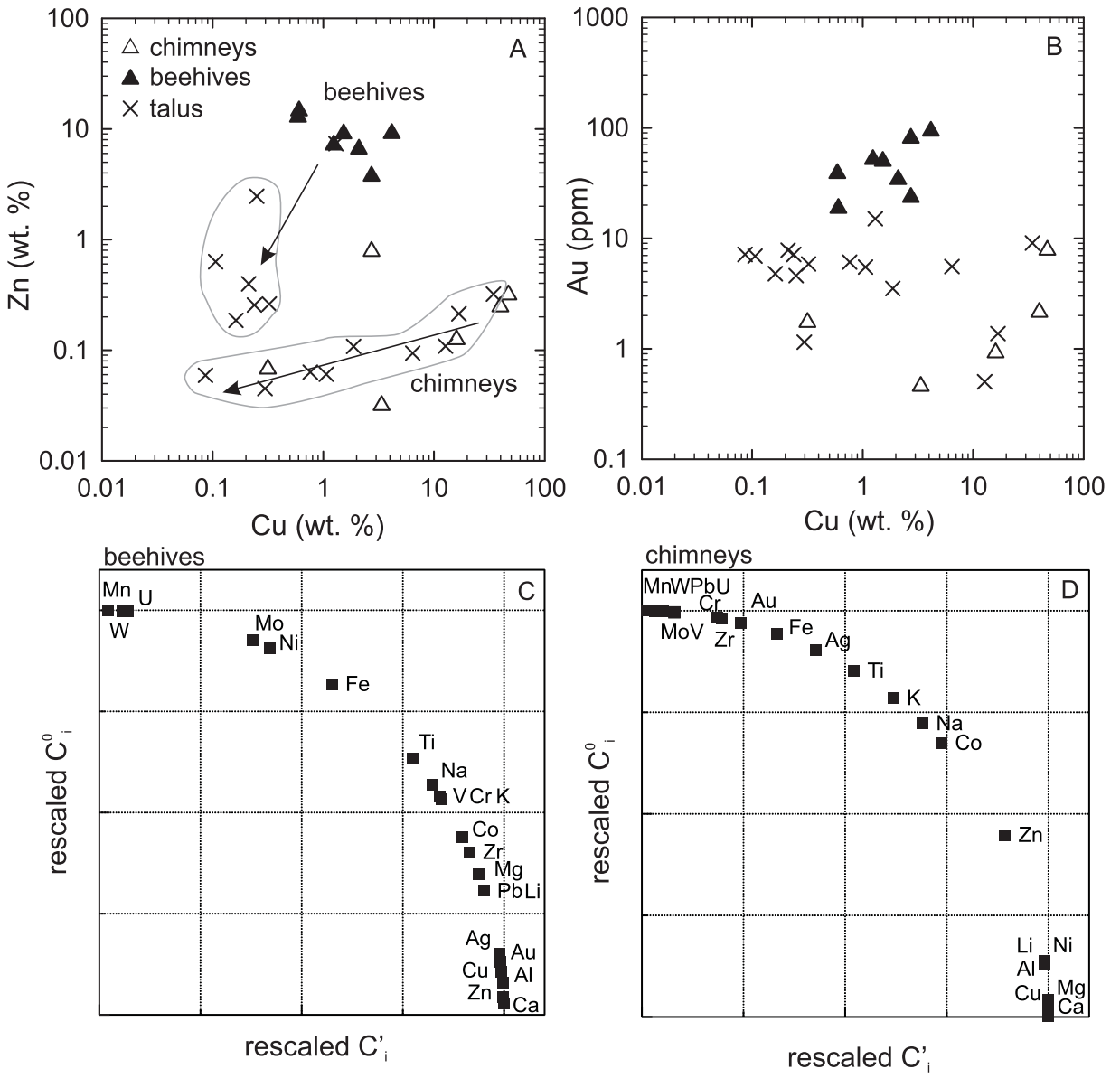

Figure 9. Assessing the degree of mobility of gold in the sulfide talus. (a) Grouping talus samples based on Cu/Zn ratio indicates which style of vent they were formed at; beehives or chimneys. This grouping was used to separate the samples into their respective protolith groups for the isocon plots. (b) Plotting Au against Cu shows that the high-temperature chimneys are relatively Cu-rich and Au-poor compared to the beehive chimneys, while the talus samples have highly variable Au concentrations. (c, d) Scaled isocon diagrams (following *Humphris et al.* [1998]) of selected elements for beehive and focused chimney talus samples, respectively. These diagrams compare the concentration of an element in the original material (C'i) with that in the altered material (C^0i), with each element scaled to allow easy visual comparison. Low C^0i/C'i indicate loss of that element, whereas a high ratio indicates gain. (b) Samples with a low Cu/Zn ratio, and therefore are likely to have originated at beehives, show gold plotting as highly mobile, along with Ca, Cu, Zn, Al, and Ag. (c) In contrast, for the samples with high Cu/Zn, Au plots as immobile, along with Mn, W, Pb, Mo, Cr, U, and Zr.

barren pyrite lens due to the lack of base metals. This may be equivalent to gold-rich pyritic bodies observed in ancient VMS deposits [e.g., *Poulson and Hannington*, 1996].

4.4. Origin of High Gold

At the BVF, gold precipitation is strongly controlled by beehive chimney formation, but other chimney types are relatively gold-rich too, and while beehives are important in trapping gold in the deposit, it cannot be the underlying control on the high gold content. Similar to other high-gold mid-ocean ridge vent sites, it does not share recognized characteristics with high-gold VMS deposits in the geological record where the auriferous deposits are generally associated with an arc setting, bi-modality in host-rock composition or continuous magmatic suites, shallow formation leading to boiling, or some other "special" characteristic

Table 3. Auriferous Volcanogenic Massive Sulfide Deposits by Host-Rock Lithology[a]

Deposit Type	n	Auriferous	Other	% Auriferous
Bimodal-Mafic	172	11	161	6.4%
Felsic	300	22	278	7.3%
Mafic	69	7	62	10.1%

[a]VMS deposits can be separated into groups based on their host-rock composition. Doing so reveals a greater proportion of mafic-hosted deposits are auriferous compared to other types. Data from USGS, available on at http://mrdata.usgs.gov/vms/.

that sets it apart from neighboring deposits [*Hannington et al*., 1995; *Dubé et al*., 2007; *Mercier-Langevin et al*., 2011, 2015]. That these high-gold, mid-ocean ridge deposits have not been recognized in the geological record is probably a function of their low preservation potential compared to arc systems. Despite this, the data for global VMS deposits show that a larger proportion of mafic-hosted systems are auriferous compared to either bi-modal mafic or felsic host-rock types (Table 3), although only 11 of the 69 mafic-hosted deposits are recognized as being mid-ocean ridge deposits. On the seafloor, there is growing evidence that vent sites situated on ultraslow spreading and ultramafic crust are particularly gold-rich [*Munch et al*., 2001; *Tao et al*., 2011; *Nayak et al*., 2014; *Fouquet et al*., 2010; *Wang et al*., 2014]. The mid-Cayman spreading center is ultraslow spreading, with one of the lowest melt thicknesses in the world [*Klein and Langmuir*, 1987; *White et al*., 2001] producing an extremely thin mafic crust just a few hundred meters thick [*Stroup and Fox*, 1981; *ten Brink et al*., 2002]. However, silica geothermobarometry indicates that the depth of hydrothermal circulation may be ~1.8 km [*Webber et al*., 2015], much deeper than the inferred thickness of basaltic crust. This low crustal thickness and depth of hydrothermal circulation, together with indications from the sulfide geochemistry [*Webber et al*., 2015] and H_2 content of the fluids [*Seewald et al*., 2012], suggest that ultramafic lithologies may be present in the reaction zone beneath the BVF. The upper mantle is generally richer in gold than MORB, with average MORB having a gold value of 0.34 ppb [*Webber et al*., 2013] compared to the upper mantle value of ~1 ppb [*Salters and Stracke*, 2004]. Gold is likely to be present in accessory sulfide grains within the ultramafic lithologies, since the partition coefficient of gold between sulfide and silicate melt is ~15,000 [*Peach et al*., 1990]. Therefore, scavenging gold from gold-rich sulfide grains within ultramafic lithologies in the reaction zone below the BVF may be a source of gold, particularly given the efficient nature of this process [*Patten et al*., 2016].

The BVF vent fluid shows clear evidence for being the low-salinity vapor phase of a supercritical, phase-separated hydrothermal fluid, with a salinity lower than that of seawater (362 mmol kg^{-1}). The behavior of gold during this process is unclear, and any conclusive analysis is prevented by the lack of a gold end-member value for the BVF and other black smoker vent fluids. However, there is some suggestion that gold is preferentially partitioned into the vapor phase in other hydrothermal systems [*Pokrovski et al*., 2014, and references therein] and it may be that this process plays a role at the BVF.

5. Conclusions

The highest gold concentrations at the BVF are controlled by the formation of beehive chimneys, which produce a highly porous pyrrhotite framework allowing for slow effusion and cooling of vent fluid. The prevalence of pyrrhotite in the samples, association with gold inclusions, and the geochemical modeling suggest gold precipitates under reduced conditions at temperatures around 130–140°C. These conditions are readily produced within beehive chimneys, which keep the fluid highly reduced by buffering with pyrite and pyrrhotite, and allow the ingress of seawater to cool the fluid. In contrast, high-temperature chimneys with relatively impermeable walls and a single orifice maintain high temperatures to the primary vent orifice, and so a much larger proportion of the gold is lost to the ocean.

The gold content of the deposit is partially controlled by alteration of chimney fragments during mass-wasting. Gold appears to be lost during this process, most prevalently from sulfide formed at beehive chimneys.

The high gold concentrations found in all chimney samples at the BVF suggest an underlying reason for high gold. Observations including a thin basaltic crust, together with penetration of hydrothermal fluids to ~1.6 km [*Webber et al*., 2015], suggest mantle peridotite as a likely source of gold compared to basalt.

Acknowledgments
This study was funded by the Natural Environment Research Council (NERC), UK (grant NE/I01442X/1). We gratefully acknowledge NERC staff and scientists aboard the RRS James Cook. We thank the reviewers Patrick Mercier-Langevin and Clifford Patten for their thorough and helpful comments. Readers can find detailed sulfide geochemistry and fluid chemistry plots in supporting information.

References

Akinfiev, N. N., and A. V. Zotov (2010), Thermodynamic description of aqueous species in the system Cu-Ag-Au-S-O-H at temperatures of 0–600°C and pressures of 1–3000 bar, *Geochem. Int.*, *48*(7), 714–720.

Benning, L. G., and T. M. Seward (1996), Hydrosulphide complexing of Au(I) in hydrothermal solutions from 150–400°C and 500–1500 bar, *Geochim. Cosmochim. Acta*, *60*(11), 1849–1871.

Cleverley, J. S., and E. N. Bastrakov (2005), K2GWB: Utility for generating thermodynamic data files for The Geochemist's Workbench (R) at 0–1000°C and 1–5000 bar from UT2K and the UNITHERM database, *Comput. Geosci.*, *31*(6), 756–767.

Connelly, D. P., et al. (2012), Hydrothermal vent fields and chemosynthetic biota on the world's deepest seafloor spreading centre, *Nat. Commun.*, *3*, 620.

Dubé, B., P. Gosselin, P. Mercier-Langevin, M. Hannington, and A. Galley (2007), Gold-rich volcanogenic massive sulphide deposits, *Geol. Assoc. Can. Spec. Pap.*, *5*, 75–94.

Eldridge, C. S., P. B. J. Barton, and H. Ohmoto (1983), Mineral textures and their bearing on the formation of the Kuroko orebodies, *Econ. Geol. Monogr.*, *5*, 241–281.

Fouquet, Y., A. Wafik, P. Cambon, C. Mevel, G. Meyer, and P. Gente (1993), Tectonic setting and mineralogical and geochemical zonation in the Snake Pit sulfide deposit (mid-Atlantic Ridge at 23°N), *Econ. Geol. Bull. Soc.*, *88*(8), 2018–2036.

Fouquet, Y., et al. (2010), Geodiversity of hydrothermal processes along the mid-Atlantic Ridge and ultramafic-hosted mineralization: A new type of oceanic Cu-Zn-Co-Au volcanogenic massive sulfide deposit, *Geophys. Monogr. Ser.*, *188*, 321–367.

Franklin, J. M., J. W. Lydon, and D. F. Sangster (1981), Volcanic-associated massive sulfide deposits, *Econ. Geol.*, *75*, 485–627.

Galley, A. G., M. Hannington, and I. Jonasson (2007), Volcanogenic massive sulphide deposits, *Geol. Assoc. Can. Spec. Pap.*, *5*, 141–161.

Hannington, M. D., and S. D. Scott (1989a), Sulfidation equilibria as guides to gold mineralization in volcanogenic massive sulfides—Evidence from sulfide mineralogy and the composition of sphalerite, *Econ. Geol.*, *84*(7), 1978–1995.

Hannington, M. D., and S. D. Scott (1989b), Gold mineralization in volcanogenic massive sulfides: Implications of data from active hydrothermal vents on the modern seafloor, *Econ. Geol.*, *6*, 491–507.

Hannington, M. D., J. M. Peter, and S. D. Scott (1986), Gold in sea-floor polymetallic sulfide deposits, *Econ. Geol.*, *81*(8), 1867–1883.

Hannington, M. D., G. Thompson, P. A. Rona, and S. D. Scott (1988), Gold and native copper in supergene sulfides from the mid-Atlantic Ridge, *Nature*, *333*(6168), 64–66.

Hannington, M. D., M. K. Tivey, A. C. L. Larocque, S. Petersen, and P. A. Rona (1995), The occurrence of gold in sulfide deposits of the TAG hydrothermal field, mid-Atlantic Ridge, *Can. Mineral.*, *33*, 1285–1310.

Hannington, M. D., K. H. Poulson, J. F. H. Thompson, and R. H. Sillitoe (1999), Volcanogenic gold in the massive sulfide environment, *Rev. Econ. Geol.*, *8*, 325–356.

Hannington, M. D., C. D. de Ronde, and S. Petersen (2005), Sea-floor tectonics and submarine hydrothermal systems, *Econ. Geol.*, *100*, 111–141.

Hekinian, R., and Y. Fouquet (1985), Volcanism and metallogenesis of axial and off-axial structures on the East Pacific Rise near 13°N, *Econ. Geol.*, *80*(2), 221–249.

Hekinian, R., J. Francheteau, and R. D. Ballard (1985), Morphology and evolution of hydrothermal deposits at the axis of the East Pacific Rise, *Oceanol. Acta*, *8*(2), 147–155.

Herzig, P. M., M. D. Hannington, Y. Fouquet, U. Vonstackelberg, and S. Petersen (1993), Gold-rich polymetallic sulfides from the Lau back-arc and implications for the geochemistry of gold in sea-floor hydrothermal systems of the Southwest Pacific, *Econ. Geol. Bull. Soc.*, *88*(8), 2182–2209.

Humphris, S. E., J. C. Alt, D. A. Teagle, and J. J. Honnorez (1998), Geochemical changes during hydrothermal alteration of basement in the stockwork beneath the active TAG hydrothermal mound, in *Proceedings of Ocean Drilling Program Scientific Results*, vol. 158, Ocean Drill. Program, College Station, Tex.

Huston, D. L. (2000), Gold in volcanic-hosted massive sulfide deposits: Distribution, genesis, and exploration, in Gold in 2000, *Rev. Econ. Geol.*, *13*, 401–426.

Huston, D. L., and R. R. Large (1989), A chemical model for the concentration of gold in volcanogenic massive sulphide deposits, *Ore Geol. Rev.*, *4*(3), 171–200.

Ihle, T., S. Petersen, P. M. Herzig, and M. D. Hannington (2005), Siting of gold and characteristics of gold-bearing massive sulfides from the interior of the felsic-hosted PACMANUS massive sulfide deposit, eastern Manus basin (PNG), in *Mineral Deposit Research: Meeting the Global Challenge*, vol. 1–2, pp. 623–626, Springer, Berlin.

Johnson, J. W., E. H. Oelkers, and H. C. Helgeson (1992), Supcrt92—A software package for calculating the standard molal thermodynamic properties of minerals, gases, aqueous species, and reactions from 1 bar to 5000 bar and 0°C to 1000°C, *Comput. Geosci.*, *18*(7), 899–947.

Jupp, T., and A. Schultz (2000), A thermodynamic explanation for black smoker temperatures, *Nature*, *403*(6772), 880–883.

Klein, E. M., and C. H. Langmuir (1987), Global correlations of ocean ridge basalt chemistry with axial depth and crustal thickness, *J. Geophys. Res.*, *92*(B8), 8089–8115.

Kong, X. Z., B. M. Tutolo, and M. O. Saar (2013), DBCreate: A SUPCRT92-based program for producing EQ3/6, TOUGHREACT, and GWB thermodynamic databases at user-defined T and P, *Comput. Geosci.*, *51*, 415–417.

Mercier-Langevin, P., M. D. Hannington, B. Dube, and V. Becu (2011), The gold content of volcanogenic massive sulfide deposits, *Miner. Deposita*, *46*(5–6), 509–539.

Mercier-Langevin, P., M. D. Hannington, D. Benoît, S. J. Piercey, J. M. Peter, and S. J. Pehrsson (2015), Precious metal enrichment processes in volcanogenic massive sulphide deposits—A summary of key features, with an emphasis on TGI-4 research contributions, *Geol. Surv. Can. Open File Rep.*, *7853*, 117–130.

Munch, U., C. Lalou, P. Halbach, and H. Fujimoto (2001), Relict hydrothermal events along the super-slow Southwest Indian spreading ridge near 63°56′E—Mineralogy, chemistry and chronology of sulfide samples, *Chem. Geol.*, *177*(3–4), 341–349.

Nayak, B., P. Halbach, B. Pracejus, and U. Munch (2014), Massive sulfides of Mount Jourdanne along the super-slow spreading Southwest Indian Ridge and their genesis, *Ore Geol. Rev.*, *63*, 115–128.

Patten, C. G., I. K. Pitcairn, D. A. Teagle, and M. Harris (2016), Mobility of Au and related elements during the hydrothermal alteration of the oceanic crust: Implications for the sources of metals in VMS deposits, *Miner. Deposita*, *51*, 179–200.

Peach, C. L., E. A. Mathez, and R. R. Keays (1990), Sulfide melt silicate melt distribution coefficients for noble-metals and other chalcophile elements as deduced from Morb—Implications for partial melting, *Geochim. Cosmochim. Acta*, *54*(12), 3379–3389.

Pokrovski, G. S., N. N. Akinfiev, A. Y. Borisova, A. V. Zotov, and K. Kouzmanov (2014), Gold speciation and transport in geological fluids: Insights from experiments and physical-chemical modelling, *Geol. Soc. Spec. Publ.*, *402*(1), 9–70.

Poulson, K. H., and M. D. Hannington (1996), Volcanic-associated massive sulphide gold, in *Geology of Canadian Mineral Deposit Types*, edited by O. R. Eckstrand, W. D. Sinclair, and R. I. Thorpe, vol. 8, pp. 183–196, Geol. Surv. of Can.

Salters, V. J. M., and A. Stracke (2004), Composition of the depleted mantle, *Geochem. Geophys. Geosyst.*, *5*, Q05B07, doi:10.1029/2003GC000597.

Seewald, J., J. McDermott, C. German, S. Sylva, E. Reeves, and F. Klein (2012), Geochemistry of hydrothermal fluids from the ultra-slow spreading mid-Cayman Rise, Abstract #OS22B-06 presented at 2012 Fall Meeting, AGU, San Francisco, Calif.

Seward, T. M., and H. L. Barnes (1997), Metal transport by hydrothermal ore fluids, in *Geochemistry of Hydrothermal Ore Deposits*, edited by H. L. Barnes, pp. 435–486, John Wiley, New York.

Stefansson, A., and T. M. Seward (2004), Gold(I) complexing in aqueous sulphide solutions to 500°C at 500 bar, *Geochim. Cosmochim. Acta*, *68*(20), 4121–4143.

Stroup, J. B., and P. J. Fox (1981), Geologic investigations in the Cayman Trough—Evidence for thin oceanic-crust along the mid-Cayman Rise, *J. Geol.*, *89*(4), 395–420.

Tao, C. H., H. M. Li, W. Huang, X. Q. Han, G. H. Wu, X. Su, N. Zhou, J. Lin, Y. H. He, and J. P. Zhou (2011), Mineralogical and geochemical features of sulfide chimneys from the 49°39′E hydrothermal field on the Southwest Indian Ridge and their geological inferences, *Chin. Sci. Bull.*, *56*(26), 2828–2838.

ten Brink, U. S., D. F. Coleman, and W. P. Dillon (2002), The nature of the crust under Cayman Trough from gravity, *Mar. Petrol. Geol.*, *19*(8), 971–987.

Thompson, G., S. E. Humphris, B. Schroeder, M. Sulanowska, and P. A. Rona (1988), Active vents and massive sulfides at 26°N (Tag) and 23°N (Snakepit) on the mid-Atlantic Ridge, *Can. Mineral.*, *26*, 697–711.

Von Damm, K. L., J. M. Edmond, B. Grant, and C. I. Measures (1985), Chemistry of Submarine Hydrothermal Solutions at 21-Degrees-N, East Pacific Rise, *Geochim Cosmochim Ac*, *49*(11), 2197–2220.

Wang, Y. J., X. Q. Han, S. Petersen, X. L. Jin, Z. Y. Qiu, and J. H. Zhu (2014), Mineralogy and geochemistry of hydrothermal precipitates from Kairei hydrothermal field, Central Indian Ridge, *Mar. Geol.*, *354*, 69–80.

Webber, A. P., S. Roberts, R. N. Taylor, and I. K. Pitcairn (2013), Golden plumes: Substantial gold enrichment of oceanic crust during ridge-plume interaction, *Geology*, *41*(1), 87–90.

Webber, A. P., S. Roberts, B. J. Murton, and M. R. S. Hodgkinson (2015), Geology, sulfide geochemistry and supercritical venting at the Beebe Hydrothermal Vent Field, Cayman Trough, *Geochem. Geophys. Geosyst.*, *16*, 2661–2678, doi:10.1002/2015GC005879.

Wheeler, A. J., et al. (2013), Moytirra: Discovery of the first known deep-sea hydrothermal vent field on the slow-spreading mid-Atlantic Ridge north of the Azores, *Geochem. Geophys. Geosyst.*, *14*, 4170–4184, doi:10.1002/ggge.20243.

White, R. S., T. A. Minshull, M. J. Bickle, and C. J. Robinson (2001), Melt generation at very slow-spreading oceanic ridges: Constraints from geochemical and geophysical data, *J. Petrol.*, *42*(6), 1171–1196.